Sea-Ice Kinematics as Determined by Remotely-Sensed Ice Drift: Seasonal Space and Time Scales

James K. Lewis and *Maria R. Giuffrida*
Science Applications International Corporation, 1304 Deacon, College Station, TX 77840

ABSTRACT: Seasonal time histories of ice motion parameters were calculated for various regions in the arctic using position data during May, August, and November of 1979. The motion of the sea ice was considered in terms of divergence, vorticity, deformation rate, and ice translation speed. These ice kinematic parameters (IKP) are determined based on the motion of ice parcels defined by drifters clustered in small regions in the arctic. The results were used to quantify seasonal space and time scales. The calculations indicate that the divergence was the most temporally and spatially variable of the IKP for all seasons. Translation speed was the most consistent in space and time. It was found that significant variations in divergence occurred in some areas on the order of 100 km and with an *e*-folding time of ~2 hours. In contrast, significant variations in the translation speed occurred in some areas on the order of 700 km and with a time scale of over 80 hours.

The small time scale of the ice pack divergence is a reflection of gravitational and buoyancy forces. These do not allow for any long term (4 to 5 days) variations in the divergence, a characteristic not reflected by the other IKP. The small space scale of the ice pack divergence is shown to be a direct result of its short time scale. These results give a number of implications for the modeling of sea ice in the arctic. The first is the need for horizontal pressure gradient terms in the model equations to account for gravitational and buoyancy forces. Others deal with limitations on the grid size and time step of arctic sea ice models.

INTRODUCTION

THE ARCTIC is a principal area for ice research because of its role in the global climate and heat budget and its economical resources. Because man's scientific and economical interests in the arctic have grown, knowledge and prediction of sea-ice conditions and the ability to cope with them have become essential. Accurate forecasting of sea-ice behavior, for example, is indispensable to research and offshore exploration. As a result, much research has been aimed at understanding the processes affecting sea ice and its distribution in the arctic.

In order to prepare for specific conditions in an environment, one must determine the modes of motion in that environment. Kinematic analysis is one of the most basic methods of defining sea-ice processes. The basic modes of motion for a parcel of ice are translation, divergence (area change), vorticity (rotation rate), and deformation (related to shape changes). These ice kinematic parameters (IKP) are particularly important in an ice-infested environment due to the variations in sea-ice loading that each variable causes. Also, the IKP are related to other important physical phenomena. For example, ice convergence is associated with ridging, which can produce thick multi-year ice floes and much under-ice noise. Ice divergence is also associated with lead formation, which can greatly modify polar atmospheric heat fluxes.

Our knowledge of sea-ice processes and ice kinematics has been substantially enhanced over the last 5 or 10 years. A great amount of research in this area has already been performed in the arctic, and these studies have provided valuable insights into ice motion and related phenomena. Hibler (1974) used kinematic analysis results to point out that sea ice tends to diverge under atmospheric lows during summer but converge under lows during winter. McPhee (1978) used kinematic analysis to quantify lower frequency ice divergence, rotation, and deformation rates in the Beaufort Sea. Similar calculations by Popelar and Kouba (1983) using positions of ice camps in the central arctic showed major changes in the ice pack deformation as the camps passed over the Lomonosov Ridge. Most recently, Lewis and Denner (1988) related under-ice arctic ambient noise variations to sea ice kinematics as determined from satellite-tracked drifters on the ice.

The results of such kinematic analyses have been very general in character. Research activities in the arctic now require a more detailed knowledge of a given parameter and its variations. Therefore, a critical need exists to establish the time and space scales over which sea ice and sea-ice processes vary. These scales indicate the coherency of a parameter both in time at a given location and in space within a given season. The scales are a function of ice characteristics and of the response of ice to particular forcings. As the characteristics of ice and/or forcing vary, so do the associated scales. As such, one might expect to observe seasonal and regional variations in the scales. Such scales are important in aiding in the set up and/or verification of numerical simulations of ice motion, establishing design criteria, and guidance in developing future studies and monitoring systems. Space and time scales can also be important in determining ice characteristics and the relative importance of various modes of ice motion in a region. Knowledge of space and time scales can be used to distinguish regions of similar ice motion characteristics.

To date, few studies of space and time scales of sea-ice processes in the arctic have been performed. With respect to space scales, Colony and Thorndike (1980) calculated the coherence of summer ice speed in the Beaufort Sea. Considering the spatial variability of summer ice movement, they found that synoptic ice motion on the scale of ~100 km was highly coherent (squared coherence of ~0.9). The coherency of inertial ice motion was of the order of 0.65.

The only study of space and time scales using data from throughout the arctic was performed by Thorndike (1986). He used 1979 ice velocity data for the central arctic basin, and the results are given in Figure 1 and Table 1. One sees that the temporal correlation of the speed components falls to about 0.7 after one day, 0.4 after two days, and decreases slowly at longer lags (Figure 1). The spatial autocorrelation of velocity (Table 1) shows a relatively high coherency out to 200 km.

PHOTOGRAMMETRIC ENGINEERING AND REMOTE SENSING,
Vol. 55, No. 8, August 1989, pp. 1113–1121.

0099-1112/89/5508–1113$02.25/0

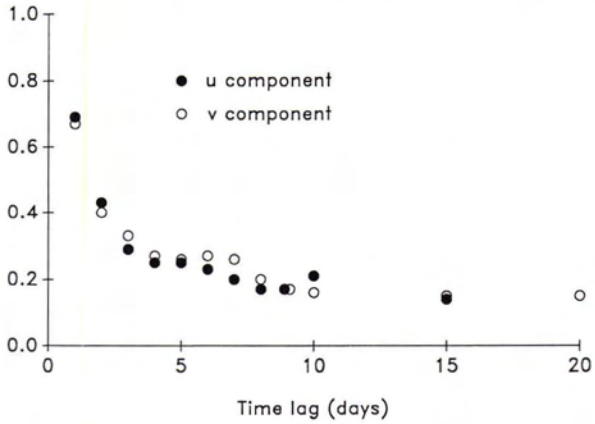

FIG. 1. Temporal autocorrelation for 1979 buoys (from Thorndike, 1986).

TABLE 1. SPATIAL CORRELATION FUNCTIONS FOR SEA-ICE VELOCITY (FROM THORNDIKE, 1986). B| |(R) IS THE CORRELATION BETWEEN THE COMPONENTS OF VELOCITY PARALLEL TO THE LINE JOINING TWO POINTS SEPARATED BY A DISTANCE R. B⊥(R) IS THE CORRELATION BETWEEN THE COMPONENTS OF VELOCITY PERPENDICULAR TO THAT LINE.

Distance (km)	B| |	B⊥
0	1.00	1.00
100	0.98	0.95
200	0.91	0.84
400	0.68	0.51
800	0.37	0.06
1200	0.19	−0.09
1600	0.10	−0.10
2000	0.01	−0.06
2400	0.00	0.00

In this study, we consider space and time scales in a more detailed fashion by working with the individual IKP and considering seasonal variations. Arctic pack-ice kinematics were determined based on the motion of ice parcels. Position data from buoys drifting on ice were used to calculate seasonal time histories of the IKP for regions covering a large portion of the arctic. This was done using May, August, and November buoy position data from 1979. The study areas covered by the data range in size from ~180 × 10^3 km² in the fall to ~270 × 10^3 km² in the spring. The IKP time histories were then used to calculate seasonal space and time scales for the translation speed, divergence, vorticity, and deformation rate in the corresponding study regions.

DATA

As part of the United States' contribution to the First GARP Global Experiment, an array of automatic data buoys was deployed in the arctic early in 1979. The data transmitted by the buoys were received by the TIROS-N and NOAA-A satellites, retransmitted to receiving stations on Earth, and relayed to Service Argos in Toulouse, France. The data used in this study include the time histories of the positions of those drifting buoys with an assumed rms position error of 500 m. Position data during May, August, and November 1979 were chosen to represent spring, summer, and fall conditions, respectively. The study areas were delineated only by those buoys which transmitted data during the entire months of May, August, and November. (Unfortunately, the position data for the winters of 1979 and 1980 were too sparse and too widely separated to adequately compose a study region for that season.)

The approximate areas of the regions delimited by the buoys during spring (15 buoys), summer (15 buoys), and fall (13 buoys) are shown in Figure 2. The coordinate system has its origin at the North Pole, its x axis coincident with the Greenwich meridian, and its y axis coincident with the 90°E meridian. Average times between position fixes for all the buoys ranged between 2 and 3 hours. Time histories of the u and v velocity components were calculated for each buoy comprising the study area. This was done to test for anomalously large velocity or acceleration values, indicators of erroneous position data. Spurious data points were eliminated. A spline fit was then performed on the position data to obtain fixes at three-hour intervals during May, August, and November 1979. These data were then used in the kinematic calculations.

CALCULATION TECHNIQUES

ICE KINEMATICS

Within each study area, the population of buoys was large enough to form a number of regions, each containing at least four buoys. These areas ranged in size from ~16 × 10^3 km² to ~62 × 10^3 km². The spring, summer, and fall study areas were partitioned into 18, 15, and 11 regions (or ice parcels), respectively. The 3-hour position data of each buoy were used to calculate the time histories of the IKP. The model used to calculate the IKP was developed following Molinari and Kirwan (1975) and Okubo and Ebbesmeyer (1976) (see Appendix).

The independent components of motion for a parcel of ice are translation (U), divergence (D), vorticity (ζ), and deformation rate (T). These IKP are defined schematically and mathematically in Fig. 3 and are interpreted as follows:

- U — the net displacement per unit time of the parcel,
- ζ — the change in the orientation of the parcel (without a shape or size change),
- D — the change in the size of the parcel (without an orientation or shape change), and
- T — the change in the shape of the parcel (without a size or orientation change).

The last three parameters are referred to as the differential kinematic parameters (DKP) and describe relative motion within the ice parcel as it translates. In this study, U is defined as the speed at which the ice parcel translates: $(u^2+v^2)^{1/2}$, where u and v are the components of the ice parcel translation velocity. The deformation rate parameter T represents the shape change rate of the ice parcel due to forces acting normal to the sides of the parcel (normal deformation rate) as well as forces acting parallel to the sides of the parcel (shear deformation rate).

We note that the mathematical definitions of the ice kinematic parameters given in Figure 3 involve line integrals along the perimeters of the ice parcels. As discussed by Thorndike (1986), such definitions represent spatial averages of the kinematic parameters over the ice parcel. Thus, the kinematic parameters represent large-scale average divergence, vorticity, and deformation of the ice. We are forced to use such definitions because sea ice is formed from an aggregate of rigid floes, and velocity gradients, in the classical sense, are not continuous. The large-scale average kinematic parameters act as direct analogs of the kinematic parameters as defined by velocity gradients for a continuous medium. The large-scale kinematic parameters can be used to compare the responses of a sometimes highly viscous medium to the large-scale forcing of the atmosphere, the primary driving force for sea ice in the central arctic. Such comparisons have provided a number of valuable insights into sea

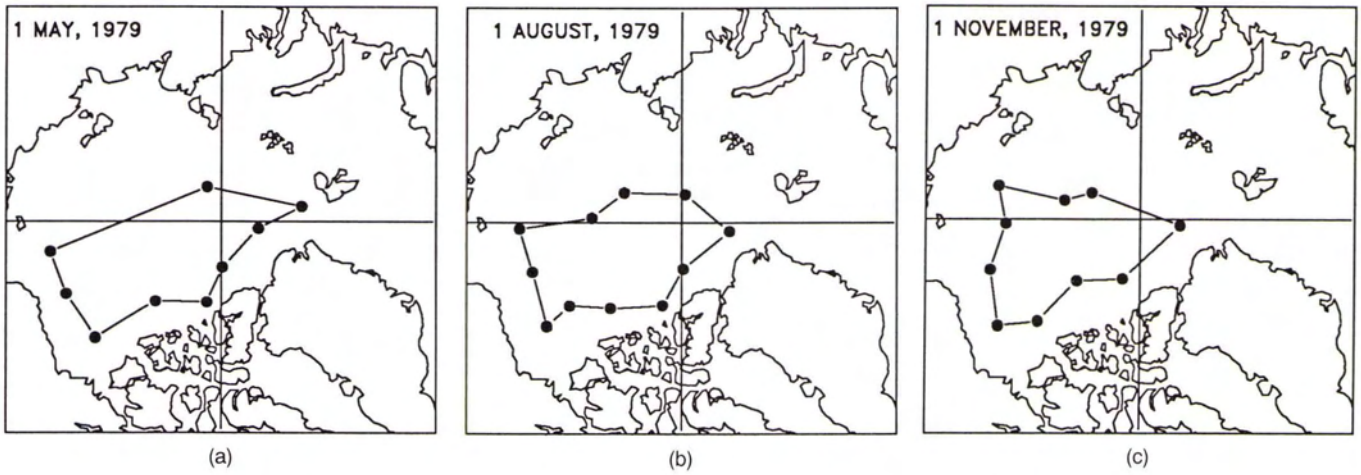

FIG. 2. Approximate study areas covered by the data for (a) May, (b) August, and (c) November of 1979. The areas are delimited using buoy positions on the first day of the month.

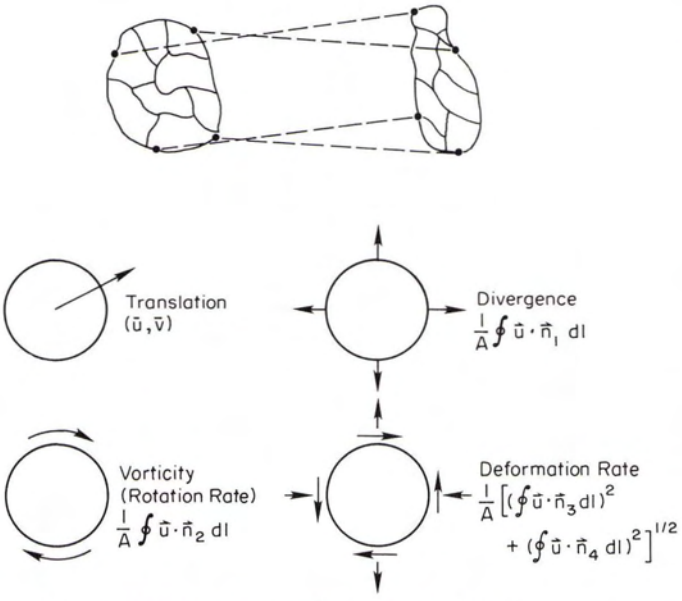

FIG. 3. Mathematical and physical definitions of the four basic components of the motion of a parcel of ice. The closed integral is about the perimeter of the ice parcel (with area A), the velocity vector is that along the perimeter, and the unit vectors n_i are the outward normal (n_1,n_2) for $i = 1$, the cyclonic parallel $(-n_2,n_1)$ for $i = 2$, $(n_1,-n_2)$ for $i = 3$, and (n_2, n_1) for $i = 4$.

ice process (e.g., Hibler, 1974; McPhee, 19787; Popelar and Kouba, 1983; Lewis and Denner, 1988).

TIME SCALES

To consider scales of temporal variations, the autocorrelations of the IKP were calculated using the spring, summer, and fall time histories. One should recall that the IKP, when used in conjunction with space and time scales, includes the speed of the ice parcel as opposed to the velocity. The time scale of the variations in the IKP was defined as that time lag at which the autocorrelation dropped to $e^{-1} = 0.36$ (e-folding scale). This allowed us to define a seasonal e-folding time, e_T, for each IKP. The e_T indicates the average time at which one could expect significant variations in the IKP at a given location and season. The e-folding time scales can be thought of in terms of persistence, with longer e-folding times implying a slower rate of change in the variable. If the calculations did not show a correlation dropping below e^{-1} for up to three days time lag (at 3-hour intervals), 80 hours was used as the e_T. In addition, each e_T was associated with the average position of the centroid of the corresponding cluster of buoys. From this information, two-dimensional contour maps of seasonal e_T's for each IKP were produced.

Time varying oscillations can be considered in terms of the magnitude of the variations and how rapidly these variations occur. The e_T's are a measure of the time scales on which these variations occur. The e_T's are a measure of the time scales on which these variations occur. In order to intercompare the e_T's, it was necessary to ensure that the magnitudes of the variations were comparable as well (i.e., of the same size). Intercomparisons of IKP time scales have little meaning when the magnitudes of the IKP variations are significantly different from one region to the next. There is the possibility that the magnitudes of the variations of ice kinematics in one region are insignificant in comparison with kinematics from other regions. In such a case, a comparison of regional e-folding scales or two-dimensional contour maps is of questionable value. To confirm that the IKP had similar magnitudes of temporal oscillations, the variances of the IKP of all the ice parcels were calculated and compared. It was found that the time-varying oscillations of the IKP for each season had similar variance magnitudes (Table 2). Thus, the time scales for the clusters can be readily intercompared.

TABLE 2. RANGES OF MAGNITUDE VARIATIONS (IN TERMS OF VARIANCES ABOUT THE MEANS) OF THE KINEMATIC PARAMETERS FOR ALL ICE PARCELS PRESENT DURING SPRING, SUMMER, AND FALL, 1979. UNITS ARE s^{-2} FOR D, T, AND ζ AND m^2/s^2 FOR U.

	Variance		
	Spring	Summer	Fall
D	$2.2 - 15.6 \times 10^{-15}$	$5.0 - 19.1 \times 10^{-15}$	$10.6 - 35.4 \times 10^{-15}$
ζ	$7.9 - 43.1 \times 10^{-15}$	$17.3 - 43.3 \times 10^{-15}$	$24.0 - 116.0 \times 10^{-15}$
T	$6.2 - 18.2 \times 10^{-15}$	$5.2 - 19.6 \times 10^{-15}$	$8.9 - 39.7 \times 10^{-15}$
U	$5.5 - 21.4 \times 10^{-4}$	$4.8 - 19.8 \times 10^{-4}$	$11.5 - 44.3 \times 10^{-4}$

Space Scales

The spatial autocorrelation of a parameter is a measure of how well the pattern of variations of the parameter is correlated with distance. However, the autocorrelation gives no indication of the magnitude of the changes of the parameter with distance. (A signal with a magnitude of 10 can be perfectly correlated with another signal of amplitude 0.1 as long as they are in phase.) Because we wanted to quantify the variations in the magnitude of the IKP, we, therefore did not use spatial autocorrelations. Instead, we considered spatial similarities of the IKP.

The spatial similarity is defined as the degree of similarity (1.0 being identical) between the values of an IKP at two locations. Let P_1 and P_2 be defined as values of an IKP at positions 1 and 2, respectively. We define the spatial similarity, S, as the average for all observations of the value

$$\text{Minimum}(|P_1|, |P_2|)/\text{Maximum}(|P_1|, |P_2|)$$

when P_1 and P_2 have the same sign. Thus, S is a measure of the average change in P (in terms of a ratio) with distance. The space scale of variations is defined as that distance at which the spatial similarity for an IKP dropped to a value of 0.6.

Because space scales are a function of ice characteristics and forcing, seasonal and regional variations of these scales were expected. Therefore, we attempted to determine regions with IKPs that had similar curves of S versus distance. However, the results suggested that distinct regions of spatial coherence within the arctic could not be defined. We, therefore, considered the entire arctic as one region in performing the seasonal space scale analysis of the IKP.

RESULTS

Time Scales

Ice pack divergence had a large temporal variability during all seasons, with the smallest e_T's being ~2 hours for each season (Table 3). During the spring, divergence had its widest range in temporal consistency, from 2.3 to 26.8 hours (Figure 4). Within the study areas, the coherency in time of the divergence appears to have generally decreased slightly from spring to fall. For all seasons, low e_T's of divergence were prevalent over the central portions of each study area. Towards the vicinity of the North Pole and the central arctic, the ice-pack divergence was more consistent in time.

Pack ice vorticity had a distinctly larger temporal coherency for all seasons than did the divergence. Vorticity time scales had a range of 8.0 to 80.0 hours from May to November. The smallest e_T for vorticity (8.0 hours) occurred during spring (Figure 5) and the largest (80.0 hours) during summer (Table 3). The temporal consistency of the vorticity within the study areas gradually increased from spring to fall. The areas of larger e_T's of ice-pack vorticity (temporally consistent) varied from one season to the next.

Temporal variations in the ice-pack deformation from May to November yielded a range of e_T's from 2.7 to 32.8 hours (Table 3). The smallest e_T occurred during fall and the largest during spring. From spring to summer, the temporal coherency of the deformation generally decreased nearly two-fold. There was then a slight increase from summer to fall. Lower e_T's of deformation occurred in the southern Beaufort Sea and the vicinity of the North Pole during spring and summer (Figure 6). However, this trend was not very pronounced. During the fall the largest e_T's of deformation occurred in the vicinity of 78°N, 158°W at the south-western edge of the study area.

From spring to fall, e_T's for the ice parcel translation speed ranged form 13.0 to 80.0 hours (Table 3). Near the North Pole, the temporal coherency of speed decreased markedly from spring to summer and then increased slightly from summer to fall. The spatial structure of the speed was similar to that of the deformation in fall and summer. During the fall, the largest e_T's occurred at the south-western edge of the study area, while the lowest values were present in the vicinity of the North Pole during the summer. However, during spring the largest e_T's of speed were found in the central arctic and near the North Pole (Figure 7).

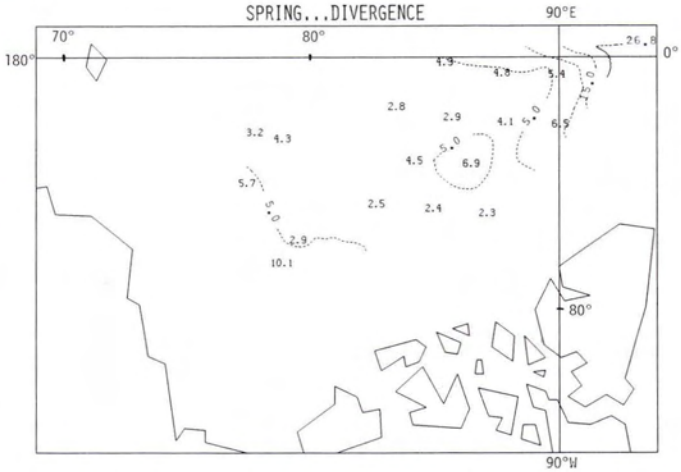

FIG. 4. Contour map of the e-folding time scales of divergence across the study area during May, 1979.

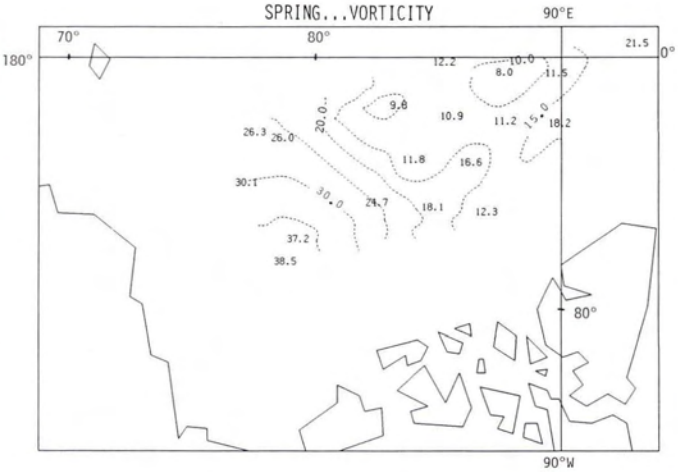

FIG. 5. Contour map of the e-folding time scales of vorticity across the study area during May, 1979.

TABLE 3. RANGE OF E-FOLDING TIMES (IN HOURS) OF EACH ICE KINEMATIC PARAMETER DURING EACH SEASON. AN E-FOLDING TIME OF 80 HOURS IMPLIES THAT THE TEMPORAL AUTOCORRELATION NEVER FELL BELOW E^{-1}.

	Spring	Summer	Fall
D	2.3 - 26.8	2.6 - 15.2	1.7 - 10.1
ζ	8.0 - 38.5	9.2 - 80.0	20.0 - 46.1
T	10.2 - 32.8	4.9 - 15.9	2.7 - 24.3
U	14.9 - 80.0	13.0 - 31.5	21.3 - 27.4

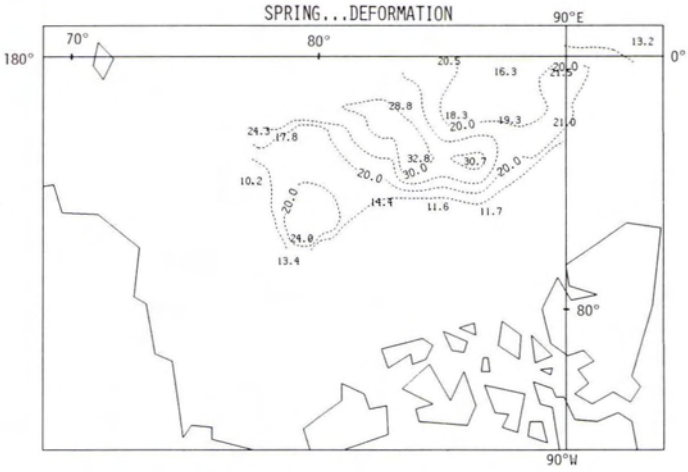

FIG. 6. Contour map of the *e*-folding time scales of deformation across the study area during May, 1979.

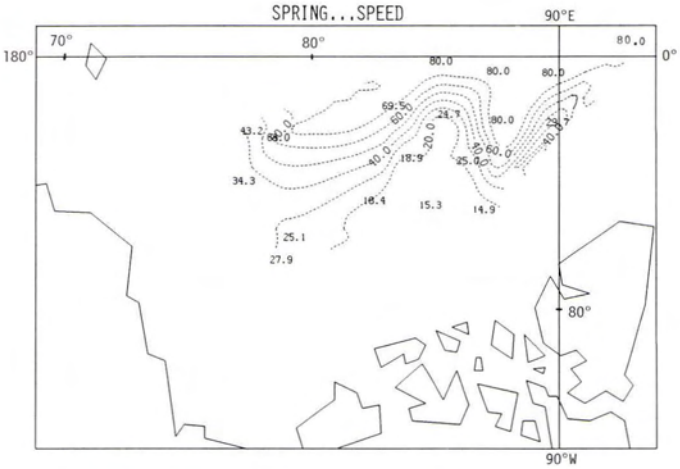

FIG. 7. Contour map of the *e*-folding time scales of speed across the study area during May, 1979.

TABLE 4. LENGTH SCALES (IN KM) OF THE ICE KINEMATIC PARAMETERS FOR EACH SEASON.

	Spring	Summer	Fall
D	195	110	160
ζ	345	280	295
T	640	520	415
U	660	705	665

SPACE SCALES

Spatial similarities of the IKP were determined as functions of distance. The length scale for each IKP is defined as that distance at which the spatial similarity fell to 0.6. These scales for each IKP and season are given in Table 4..

The length scales given in Table 4 provide interesting information on the IKP during spring, summer, and fall 1979. One sees that the ice-pack divergence had the largest spatial variability of all the kinematic parameters considered, with space scale values ranging from 100 to 200 km. The lowest similarity occurred during summer, with significant variations having a scale of ~100 km. From these results, as well as from the results of the time scale analyses, we see that the divergence is the most spatially and temporally incoherent of the IKP.

In contrast, results in Table 4 indicate that speed was the most spatially consistent of the IKP, with space scale values ranging from 650 to 700 km. During summer, the spatial similarity in speed was at its greatest value. The variabilities during the spring and fall were nearly equal and slightly smaller than those of summer. The deformation rate also had high spatial coherency, particularly during spring. The range of space scale values was from 650 km in spring to 400 km in fall. A gradual increase in spatial variability occurred from spring to fall 1979.

The vorticity had smaller length scales in comparison to those of speed and deformation rate. Values ranged from ~300 km in summer to 350 km in spring. There was an increase in spatial variability from spring to summer and then a gradual decrease from summer to fall.

An interesting point can be noted about the plots of similarity as a function of distance (Figures 8 to 10). Beyond a given distance L, the average spatial similarity for each IKP appears to be nearly constant. Thus, for a given IKP, the minimum average similarity between the IKP at two locations is reached when the locations have a separation of at least L. The value L is defined as the distance between two locations beyond which the average similarity between IKP at the locations is approximately constant and at a minimum.

We define S_{min} as the constant, minimum average similarity associated with the distance L. One sees that, for a given IKP,

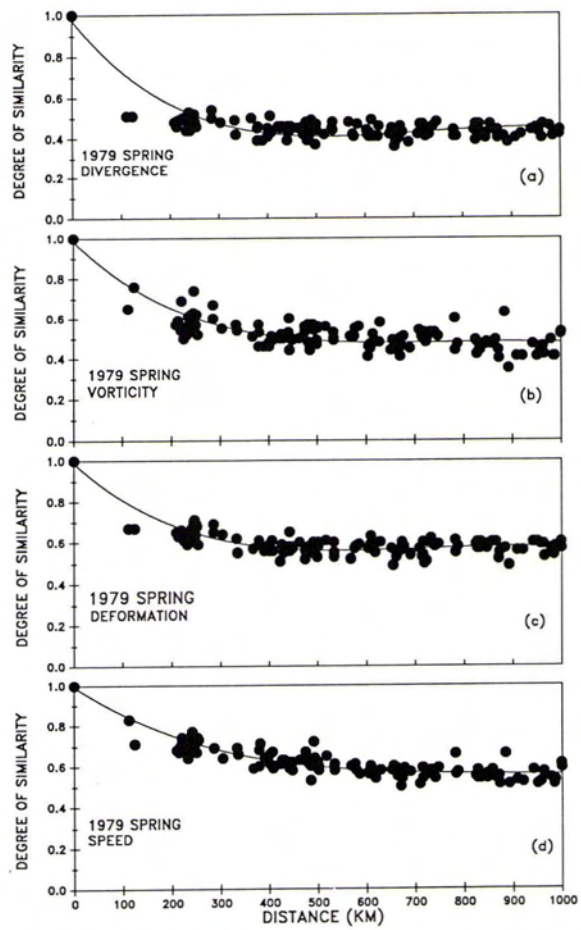

FIG. 8. Spatial similarities of (a) divergence, (b) vorticity, (c) deformation, and (d)speed as functions of distance for spring, 1979.

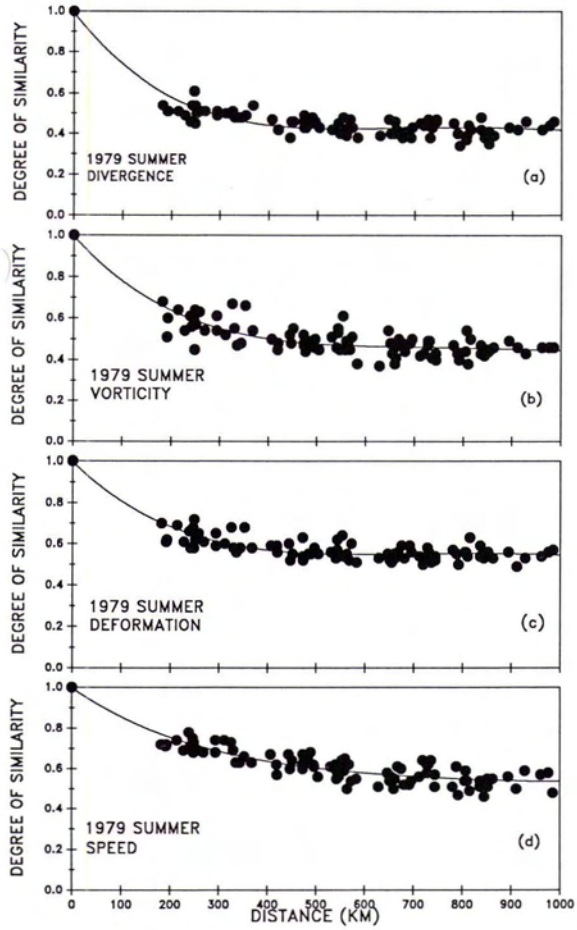

FIG. 9. Spatial similarities of (a) divergence, (b) vorticity, (c) deformation, and (d) speed as functions of distance for summer, 1979.

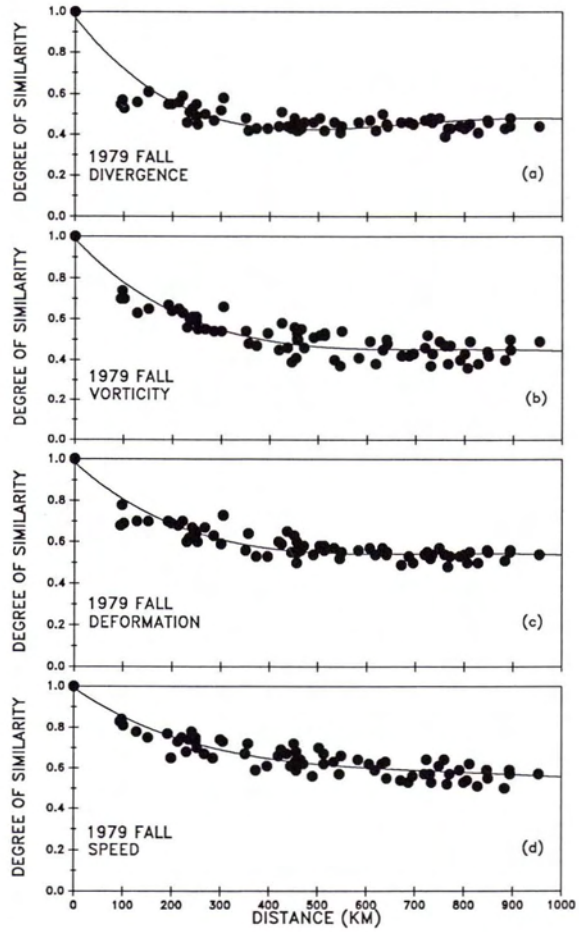

FIG. 10. Spatial similarities of (a) divergence, (b) vorticity, (c) deformation, and (d) speed as functions of distance for fall, 1979.

the S_{min}'s and the L's are nearly equivalent during spring, summer, and fall (Figures 8 to 10). For example, the S_{min} for vorticity is approximately 0.47, and the value of L is about 575 km during all seasons. Table 5 gives values of S_{min} and L for each IKP for each season.

TABLE 5. VALUES OF S_{min} AND L FOR EACH IKP DURING EACH SEASON.

		Spring	Summer	Fall
S_{min}	D	0.42	0.43	0.43
	ζ	0.48	0.47	0.46
	T	0.56	0.55	0.55
	U	0.58	0.56	0.59
L(km)	D	478	469	475
	ζ	560	575	590
	T	625	630	628
	U	810	830	849

DISCUSSION

The results of the last section indicate that ice-pack divergence had the largest temporal and spatial variability of the IKP during all seasons studied. Spatial variations in divergence ranged from only 100 to 200 km. The time scales were as low as ~2 hours. In contrast, significant variations in the translation speed occurred in some areas on the order of 700 km and over a time period as great as 80 hours. Overall, the short space and time scales of ice-pack divergence were not reflected in the other ice kinematic parameters.

TIME SCALES

One might immediately suspect that the short-term variability of pack ice divergence is a result of measurement noise. However, upon closer inspection this is seen to be unlikely. First, the methodology in calculating differential motion is one in which the bias of the position error is estimated and then removed (Kirwan and Chang, 1979). Secondly, in almost all cases only the divergence of a cluster for a given month had a short e-folding time while the vorticity and deformation had time scales that were up to 8 to 12 times longer. Finally, low pass filtering the position data (to remove position errors) had little effect on the time scale results. Data were low-pass filtered using a 10.5-hr half-power point filter that passed 95 percent of the energy at 12 hours. In general, the speed, vorticity, and deformation time scales of the filtered data were similar to those of the unfiltered data (within 10 percent). The time scales of the divergence using the filtered position data increased from 2–3 hr to 5–6 hr, still 5 to 7 times smaller than the scales of the other parameters. These factors indicate that position error is not the cause of the short time scales of ice pack divergence.

To fully understand the differences in the time scales of the IKP, we must first consider the implication of the e-folding time scales. If we are dealing with a purely sinusoidal signal, the correlation drops to e^{-1} when the sinusoid is shifted 79.4° with

respect to itself. If the period of oscillation of the sinusoid is T hours, then a 79.4° phase shift translates to a $T \times 79.4/360$ hour phase shift (approximately 22 percent of the period). Based on this simple illustration, the 2- to 3-hour time scales of pack-ice divergence would imply a signal with an average period of oscillation of 9 to 13 hours. The 20- to 25-hour time scales of the other IKP indicate oscillations on the order of 4 to 5 days. The actual implication of these time scales is seen in the spectral density of divergence, vorticity, and deformation for various regions in the arctic. An example is shown in Figure 11. These data show that we must answer the question as to why pack ice can undergo significant long-term oscillations (4 to 5 days) in deformation, rotation, and translation, but not in divergence.

The most simple explanation for such differences is the mass-conserving requirement that horizontal convergence/divergence be compensated by motion in the vertical. In the case of ice, long-period oscillations in rotation rate (vorticity) and shape changes (deformation) can be easily triggered by the passage of atmospheric fronts. But for ice to have long-period divergence/covergence, there must be compensating long-period oscillations in ridge building and keel formation.

Ridge building and keel formation are processes that include the overcoming of (1) the compressive strength of the pack ice, (2) the retarding force of gravity, and (3) the buoyancy forces of the denser sea water. A convergent ice field may fracture the ice, but additional energy is required to push the fractured floes upward against gravity or downward into the ocean. As a ridge or keel grows larger, the restoring forces of buoyancy and gravity become greater. Thus, long-term oscillations in ice-pack divergence would imply long-term upward and downward motion and, essentially, mountainous ice structures. Of course, buoyancy/gravity restoring forces can be overcome to only a limited extent. Therefore, restrictions placed on the amount of vertical movement by the buoyancy/gravity restoring forces can result in smaller time scale oscillations for divergence and a lack of energy at low frequencies. Conversely, rotating and deformative motion are not inhibited by any vertical restoring forces and, therefore, may persist over longer periods of time.

Space Scales

The minimum length scale of pack ice divergence was calculated to be ~100 km (Table 4). This value is of the order of the distance between the ice parcels considered. Therefore, the actual minimum length scale may even be somewhat less. It is seen that other IKP have length scales 3 to 7 times as large as those associated with divergence. In our search to provide the most simple explanation for these space scale differences, we found that the short time scales of ice-pack divergence could directly cause spatial incoherency.

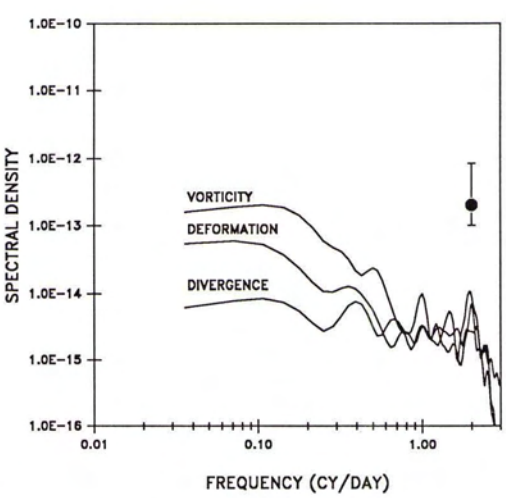

FIG. 11. Power spectra for ice divergence, vorticity, and deformation in the Beaufort Sea. Confidence intervals of 95 percent are indicated.

Consider an atmospheric disturbance, $W(t)$, which takes time T to travel length L across the ice pack. We assume that the moving troughs of such disturbances trigger various modes of responses in the ice pack. We will consider responses B and C. Responses B and C are assumed to be oscillatory and have their own time scales, T_b and T_c, respectively. Let the position of the trough of the atmospheric disturbance at time t be given by

$$X(t) = t\,L/T,\ 0 < t < T.$$

Therefore, the initiation of B and C at a point x begins at time $t = Tx/L$. Thus, for any x and t, responses B and C can be written as:

$$B(x,t) = A_b \sin\,[(t - T\,x/L)\,2\,/\,T_b]$$
$$C(x,t) = A_c \sin\,[(t - t\,x/L)\,2\,/\,T_c],$$

where A is the amplitude of the oscillation. The above expressions imply that the ice-pack responses are triggered as the trough of the disturbance passes, and they then continue to oscillate at their own natural frequency.

For convenience, we choose as a frame of reference X_o such that $t - T\,X_o/L = 0$ (i.e., B and C, are zero). Now consider the space scales L_b and L_c which are distances over which B and C, respectively, are continuously positive at time t:

Response B - positive from $X_o = t\,L/T$ to $x_b = (t - T_b/2)L/T$
Response C - positive from $X_o = t\,L/T$ to $x_c = (t - T_c/2)L/T$.

Therefore, length scales of the responses B and C are defined as

$$L_b = X_o - x_b = T_b L/2\,T$$
$$L_c = X_o - x_c = T_c L/2\,T.$$

Hence, it is shown that there is a simple one-to-one relation between the relative magnitudes of space and time scales. It follows that modes of motion triggered by a passing disturbance and having small time scales (e.g., ice-pack divergence) will also exhibit a high degree of spatial variability. And motions that are coherent in time will tend to be spatially consistent when triggered by a moving disturbance.

Finally, we comment on the parameters S_{min} and L (Table 5). The magnitudes of the S_{min} values suggest a simple explanation for this characteristic in the similarity plots. Suppose we have a variable X which is uniformly distributed over the interval (a,b). It can be shown that the mean similarity of sets of independent samples of X from the interval (a,b) has a value of 0.5. The similarities of all the IKP also tend toward a value of 0.5, but at different distances for each variable. Thus, a simple interpretation of this phenomena is that, at distances > L, the spatial variations of the IKP can be considered nearly uniformly distributed. Geophysically, this implies that L is beyond the range at which one can detect, in the mean, a distinct trend in the spatial distribution of the IKP. As expected from the space scale results, ice pack divergence has the smallest L scale, being ~475 km. The trend for larger L scales for vorticity, then deformation, and then speed is followed, with the ice speed having an L scale of ~825 km.

SUMMARY AND CONCLUSIONS

Seasonal time histories of the ice kinematic parameters were calculated using position data from drifting buoys in the arctic during May, August, and Novemeber 1979. The results were used to determine seasonal space and time scales of D, ζ, T,

and U variations in the arctic. An e-folding scale was used as a measure of the temporal coherency. Spatial variability was defined in terms of the degree of similarity between the magnitudes of a parameter at two locations.

In general, the ice-pack divergence was the most temporally and spatially variable of the IKP during spring, summer, and fall. In contrast, the translation speed showed the highest degree of temporal and spatial coherency during all seasons. The time scale calculations indicate that significant variations of some ice kinematics can occur on the order of 2 hours. The minimum time scales of divergence were of the order of the sampling interval of the drifter position data (3 hours). Thus, there is the possibility that the average minimum time scales for this parameter may actually be lower than those calculated in this study.

The short time scales of ice pack divergence are not reflected in the other IKP but can be explained by considering the buoyancy/gravity restoring forces at work in ice. These forces act to limit the size of the ice ridges and keels created in ice convergence. Ice pack divergence is, thus, a mode of motion charcterized by smaller time scale oscillations with very little energy at lower frequencies. In contrast, the other kinematic motions are not restrained by such restoring forces and, as such, can sustain long-term variations.

It is shown analytically that there can be a simple one-to-one relationship between temporal and spatial variability for a given mode of motion. Therefore, the mechanisms at work to produce the short time scales of ice-pack divergence can also be responsible for its small space scales.

There are several implications here for the modeling of arctic pack ice. The first deals with the governing equations and scales for pack ice divergence. The horizontal equations of motion should include horizontal pressure gradient terms. These terms incorporate the effects of gravitational and buoyancy forces and force the pack ice to limit its duration of convergence. In Hibler's (1979) original model formulation, only a sea surface tilt term was incorporated. A modification of the Hibler model is run operationally by the U.S. Navy, and it too lacks horizontal pressure gradient terms. Thus, we can suspect that such models will produce unreliable estimates of the time variations of pack ice divergence. And, as pointed out above, space scales are related to time scales. So we should also expect too large of a spatial coherency for divergence from these models.

Another implication of this work deals with the time step and grid size of a numerical model. If ice pack divergence is to be resolved, a minimum time step of 5 to 6 hours is required. Such a time step gives a Nyquist frequency of 10 to 12 hours (corresponding to minimum e-folding times of 2.2 to 2.6 hours). Moreover, a grid size of ~100 km is required to resolve significant spatial variations in divergence.

ACKNOWLEDGMENTS

This work was supported by the United States Navy, ASW Oceanography Program, at the Naval Oceanographic Research and Development Activity, NSTL, Mississippi. The authors appreciate the guidance and comments of Dr. Allen Thorndike in conducting this study.

REFERENCES

Colony, R., and A. S. Thorndike, 1980. The horizontal coherency of the motion of summer arctic sea ice. *J. Phys. Oceanogr.*, 10, pp. 1281–1289.

Hibler, W. D., III, 1974. Differential sea ice drift. II. Comparison of mesoscale strain measurements to linear drift theory predictions. *J. Glaciology*, 13, pp. 457–471.

———, 1979. A dynamic thermodynamic sea ice model. *J. Phys. Oceanogr.*, 9, 815–846.

Hibler, W. D., III, and W. B. Tucker, III, 1979. Some results from a linear-viscous model of the arctic-sea ice cover. *J. Glaciology*, 22(87), 293–304.

Kirwan, A. D., 1988. Notes on the cluster method for interpreting relative motions. *J. Geophys. Res.*, 93(C8), 9337–9339.

Kirwan, A. D., and M. S. Chang, 1979. Effects of sampling rate and random position error on analysis of drifter data. *J. Phys. Oceanogr.*, 9, 382–387.

Kirwan, A. D., W. J. Merrel, J. K. Lewis, R. E. Whitaker, and R. Legeckis, 1984. A model for the analysis of drifter data with an application to a warm core ring in the Gulf of Mexico. *J. Geophys. Res.*, 89 (C3), 3425–3438.

Lewis, J. K., and W. W. Denner, 1988. Arctic ambient noise in the Beaufort Sea: seasonal relationships to sea ice kinematics. *J. Acoust. Soc. Am.*, 83(2), 549–565.

McPhee, M. G., 1978. The free-drift velocity field across the AIDJEX manned camp array. *AIDJEX Bull.*, 38, pp. 158–163.

Molinari, R., and A. D. Kirwan, 1975. Calculation of differential kinematic properties of the Yucatan Current from Lagrangian observations. *J. Phys. Oceanogr.*, 5, pp. 483–491.

Okubo, A., 1970. Dispersion of floatable particles in the vicinity of velocity singularities such as convergences. *Deep Sea Res.*, 17, 445–454.

Okubo, A., and C. C. Ebbesmeyer, 1976. Determination of vorticity, divergence, and deformation rates from analysis of drogue observations. *Deep Sea Res.*, 23, pp. 349–352.

Popelar, J., and J. Kouba, 1983. Satellite Doppler determination of differential sea ice motion in the vicinity of the North Pole. *Mar. Geodesy*, 7, 171–198.

Thorndike, A. S., 1986. Kinematics of sea ice. *The Geophysics of Sea Ice* (N. Untersteiner, ed.), Plenum Press, New York, N.Y., pp. 489–549.

APPENDIX

Drifters clustered in small regions of the ocean have been used to infer characteristics of horizontal shears. A model frequently used for this purpose was developed by Molinari and Kirwan (1975) and Okubo and Ebbesmeyer (1976). The model is of the local variety. In essence, it is a Taylor's expansion for the velocity of the ith drifter in the cluster relative to some moving origin:

$$u_i = [(D + N)\, x_i]/2 + [(S - \zeta)\, y_i]/2 + f_i \qquad \text{(A1)}$$
$$v_i = [(S + \zeta)\, x_i]/2 + [(D - N)\, y_i]/2 + g_i.$$

Here the coordinates of the drifter i with respect to the origin are (x_i, y_i), D is divergence, ζ is vorticity, S is shear deformation rate, N is normal deformation rate, and (f_i, g_i) represent the sum of the higher order non-linear terms in the expansion as well as random turbulent motion. From the statistical standpoint, (f_i, g_i) represent random deviations from the model. In an absolute frame, the cluster is being translated at the absolute velocity of the origin. In a recent note, Kirwan (1988) discusses some of the limitations of this method.

Previous studies have estimated D, ζ, N, and S (the differential kinematic parameters, or DKP) by determining the (u_i, v_i) and (x_i, y_i) from absolute position data and then employing least squares. But least-squares procedures assume that the independent variables in the equations (drifter velocities and positions) are determined independently. Of course, this assumption is never true, but the analysis procedure presented in Kirwan *et al.* (1984) provides a means of overcoming this short-coming. To do this, we make explicit use of the appropriate solutions to Equation A1. The method of LaPlace Transforms gives the forms of the solutions for these coupled equations, all of which are crucially dependent on the frequency parameter

$$\gamma^2 = N^2 + S^2 - \zeta^2. \qquad \text{(A2)}$$

There are three classes of solutions depending on different val-

TABLE A1. DEFINITIONS OF THE H, J, AND K FUNCTIONS. HERE ψ REPRESENTS THE MAGNITUDE OF $(N^2 + S^2 - \zeta^2)^{1/2}$.

γ^2	$H(t)$	$J(t)$	$K(t)$
>0	$e^{Dt/2}$ (cosh $\psi t/2$ + (N/ψ) sinh $\psi t/2$)	$e^{Dt/2}$ sinh $\psi t/2$	$e^{Dt/2}$ (cosh $\psi t/2$ - (N/ψ) sinh $\psi t/2$)
$=0$	$e^{Dt/2}$ $(1 + N\ t/2)$	$(te^{Dt/2})/2$	$e^{Dt/2}$ $(1 - N\ t/2)$
<0	$e^{Dt/2}$ (cos $\psi t/2$ + (N/ψ) sin $\psi t/2$)	$e^{Dt/2}$ sin $\psi t/2$	$e^{Dt/2}$ (cos $\psi t/2$ - (N/ψ) sin $\psi t/2$)

ues of γ^2 (see Okubo (1970) for a discussion). All three can be expressed in the form

$$x_i(t) = X_i\, H(t) + Y_i\, J(t)\, (S - \zeta) + \int_0^t f_i(t - \beta)\, H(\beta)\, d\beta + (S - \zeta) \int_0^t g_i(t - \beta)\, J(\beta)\, d\beta \qquad \text{(A3)}$$

$$y_i(t) = Y_i\, K(t) + X_i\, J(t)\, (S + \zeta) + \int_0^t g_i(t - \beta)\, K(\beta)\, d\beta + (S + \zeta) \int_0^t f_i(t - \beta)\, J(\beta)\, d\beta$$

The (X_i, Y_i) are the coordinates of the ith drifter at time $t = 0$ relative to the local origin at that time.

The forms of the H, J, and K functions depend on γ^2. Table A1 summarizes the possibilities. This table shows that, when the sum of squares of the shear and normal distortion exceeds the squared vorticity ($\gamma^2 > 0$, Case I), then the drifter displacements will increase exponentially with time (for $D = 0$). For Case II, ($\gamma^2 = 0$), the solutions show that the drifter displacements will grow linearly with time (aside from the divergence term). Finally, for Case III ($\gamma^2 < 0$), the drifter trajectories relative to the origin form ellipses (for $D = 0$). When $N^2 = S^2 = 0$, these ellipses become circles.

We now note that, for appropriately short times (i.e., $Dt/2$ and $\gamma t/2 << 1$) and constant (f_i, g_i), all of the cases reduce to the approximate linear form

$$x_i = X_i + t\, [X_i\, (D + N)/2 + Y_i\, (S - \zeta)/2 + f_i] \qquad \text{(A4)}$$
$$y_i = Y_i + t\, [Y_i\, (D - N)/2 + X_i\, (S + \zeta)/2 + g_i].$$

These equations state that the present position relative to the moving origin is obtained by adding to the previous relative position the displacements due to the random velocity and to the velocity induced by the average rotation, divergence, and distortion of the cluster during the time interval. We may rewrite the first equation in Equation A4 as

$$(x_i - X_i)/t = X_i\, (D + N)/2 + Y_i\, (S - \zeta)/2 + f_i \qquad \text{(A5)}$$

which is similar in form to Equation A1. The form of Equation A5 typically used in previous studies was

$$(x_i - X_i)/t = (x_i + X_i)\, (D + N)/4 + (y_i + Y_i)\, (S - \zeta)/4 + f_i$$

where the DKP values were those associated with the time at which the drifter was at position $(x_i + X_i)/2$ and $(y_i + Y_i)/2$. Thus, the analytical solutions show that the previously used solution techniques were using an incorrect form of the Taylor's expansion.

We see that the solutions to the governing expressions provide information concerning three important factors. First, they provide a system of equations in which the only dependent variables are position and random velocity. This eliminates the problem of having two variables (position and velocity) which are not determined independently. Second, the solutions give the correct form of the Taylor's expansion to calculate the DKP. Finally, we see that we can apply the expressions in Equation A4 only if the time interval t between position fixes is such that $Dt/2$ and $\gamma t/2 << 1$. This last factor is of considerable importance. For open ocean conditions, the time step restriction is of the order of 6 hrs. But for arctic ice conditions, position fixes should be on the order of 1 day except during winter, when position fixes of once every 5 to 6 days can be used to calculate the DKP.